Monthly Notices of the ROYAL ASTRONOMICAL SOCIETY

MNRAS **461,** 542–551 (2016) doi:10.1093/mnras/stw1349
Advance Access publication 2016 June 7

Galactic planetary nebulae with precise nebular abundances as a tool to understand the evolution of asymptotic giant branch stars

D. A. García-Hernández,[1,2]★ P. Ventura,[3] G. Delgado-Inglada,[4] F. Dell'Agli,[3] M. Di Criscienzo[3] and A. Yagüe[1,2,3]

[1]*Instituto de Astrofísica de Canarias, E-38205 La Laguna, Tenerife, Spain*
[2]*Departamento de Astrofísica, Universidad de La Laguna (ULL), E-38206 La Laguna, Tenerife, Spain*
[3]*INAF - Osservatorio Astronomico di Roma, Via Frascati 33, I-00040 Monte Porzio Catone (RM), Italy*
[4]*Instituto de Astronomía, Universidad Nacional Autónoma de México, Apdo. Postal 70264, 04510 México D. F., Mexico*

Accepted 2016 June 2. Received 2016 June 1; in original form 2016 May 3

ABSTRACT

We present nucleosynthesis predictions (HeCNOCl) from asymptotic giant branch (AGB) models, with diffusive overshooting from all the convective borders, in the metallicity range $Z_{\odot}/4 < Z < 2\,Z_{\odot}$. They are compared to recent precise nebular abundances in a sample of Galactic planetary nebulae (PNe) that is divided among double-dust chemistry (DC) and oxygen-dust chemistry (OC) according to the infrared dust features. Unlike the similar subsample of Galactic carbon-dust chemistry PNe recently analysed by us, here the individual abundance errors, the higher metallicity spread, and the uncertain dust types/subtypes in some PNe do not allow a clear determination of the AGB progenitor masses (and formation epochs) for both PNe samples; the comparison is thus more focused on a object-by-object basis. The lowest metallicity OC PNe evolve from low-mass ($\sim$1 $M_{\odot}$) O-rich AGBs, while the higher metallicity ones (all with uncertain dust classifications) display a chemical pattern similar to the DC PNe. In agreement with recent literature, the DC PNe mostly descend from high-mass ($M \geq 3.5\,M_{\odot}$) solar/supersolar metallicity AGBs that experience hot bottom burning (HBB), but other formation channels in low-mass AGBs like extra mixing, stellar rotation, binary interaction, or He pre-enrichment cannot be disregarded until more accurate C/O ratios would be obtained. Two objects among the DC PNe show the imprint of advanced CNO processing and deep second dredge-up, suggesting progenitors masses close to the limit to evolve as core collapse supernovae (above $6M_{\odot}$). Their actual C/O ratio, if confirmed, indicate contamination from the third dredge-up, rejecting the hypothesis that the chemical composition of such high-metallicity massive AGBs is modified exclusively by HBB.

Key words: nuclear reactions, nucleosynthesis, abundances – stars: abundances – stars: AGB and post-AGB – planetary nebulae: general – Galaxy: abundances.

1 INTRODUCTION

All the stars of mass in the range $1\,M_{\odot} < M < 8\,M_{\odot}$, after the core He burning phase, evolve through the asymptotic giant branch (AGB) just before the planetary nebula (PN) and white dwarf phases. AGB stars are mainly supported by shell H burning but 3α nucleosynthesis is periodically activated in a He-rich layer above the degenerate core. These periodic episodes are commonly referred to as thermal pulses because the ignition of this nuclear channel occurs under condition of thermal instability (Schwarzschild & Harm 1965, 1967). The thermally pulsing (TP) phase at the end of the AGB is particularly important because nucleosynthesis primarily occurs in this evolutionary stage. During the TP-AGB phase, the so-called third dredge-up (TDU) brings the products of H and He burning to the stellar surface, increasing the C/O ratio over unity and forming C-rich AGB stars. In the more massive (say, M > 3−4 $M_{\odot}$ at solar metallicity) AGBs, the star's surface may be also enriched in N (and ^{13}C) at the expenses of ^{12}C as a consequence of hot bottom burning (HBB; e.g. Mazzitelli, D'Antona & Ventura 1999), keeping the C/O ratio below unity.

AGB stars play a significant role in several astrophysical contexts: (i) they are used to infer the masses of galaxies at high redshifts (Maraston et al. 2006) because of their large IR luminosities; (ii) they provide an important contribution to the light elements enrichment of the interstellar medium (ISM) in our Milky Way Galaxy and

★E-mail: agarcia@iac.es

© 2016 The Authors
Published by Oxford University Press on behalf of the Royal Astronomical Society

Downloaded from https://academic.oup.com/mnras/article-abstract/461/1/542/2595305 by guest on 13 June 2020

other galaxies (Romano et al. 2010) due to their high gas pollution capability via stellar winds; (iii) AGBs, because of the efficiency of the dust-formation process in their winds, play a crucial role in the formation and evolution of galaxies (Santini et al. 2014), proving essential for the understanding of the dust content in high-redshift quasars (Valiante et al. 2011); (iv) the more massive HBB AGB stars (e.g. García-Hernández et al. 2006, 2007, 2009) are currently believed to have provided the gas required to form second-generation stars in globular clusters (Ventura et al. 2001; D'Ercole et al. 2008). The above arguments represent only some examples, showing why the AGB evolutionary phase, despite lasting only a tiny fraction of the whole life of a star, is at the centre of the astrophysical debate. Addressing the aforementioned topics requires full knowledge of the AGB evolution properties, and a detailed description of the gas and dust yields provided by these objects.

AGB modelling has been significantly improved in the last few years; the last generation of AGB models also include a description of the dust-formation process (Ferrarotti & Gail 2006; Ventura et al. 2012a,b; Di Criscienzo et al. 2013; Ventura et al. 2014a; Nanni et al. 2013a,b, 2014). This opens the possibility of determining the dust produced by AGBs, in terms of the chemical composition of the dust particles formed, the dust mass budget and the grain size distribution. The reliability of the results presented so far, somewhat quantified through the differences among the model results of the different groups involved in this research, is not satisfactory though. This is primarily due to the poor knowledge of convection and mass loss, still modelled via semi-empirical descriptions and that deeply affect the results obtained (Ventura & D'Antona 2005a,b; Doherty et al. 2014a,b). Because we are still far from a self-consistent and physically sound treatment of both mechanisms, still based on first principles, the best way to make a significant step forward into this direction is the comparison between the theoretical predictions and the astronomical observations.

The chemistry of PNe is the result of the several nucleosynthesis processes that modify the stellar chemical composition during the previous AGB phase. Thus, PNe – which can be observed at large distances and the nebular gas abundances can be derived – turn out to be particularly useful objects in order to test the AGB theoretical models (Marigo et al. 2003, 2011; Stanghellini et al. 2009). Some species such as C and N (to a more limited extend O; e.g. Delgado-Inglada et al. 2015; García-Hernández et al. 2016) are greatly altered during the earlier AGB phase, while another ones like Cl remain almost constant to values typical of the original ISM. For these reasons we started a project dedicated to the comparison between the observations of PNe and the surface chemical composition of AGB models in the latest evolutionary phases, with the ultimate goal of putting additional constraints on the description of the AGB phase.

In the first two papers of this series (Ventura et al. 2015, 2016) we focused on the PNe sample of the Large and Small Magellanic Clouds (LMC and SMC); these works offered an interesting opportunity to complete, from a different perspective, the analysis focused on the interpretation of the *Spitzer* sample of AGBs in the same galaxies (Dell'Agli et al. 2014, 2015a,b). The analysis by Ventura et al. (2015, 2016), based on the observed chemical composition, particularly of the CN abundances, allowed a characterization of the PNe observed in terms of formation epoch and progenitor's metallicity and mass; this investigation provided interesting information regarding the efficiency of the processes able to alter the surface chemistry of AGBs, particularly at the low metallicities typical of the stars in the Magellanic Clouds.

In this paper we make a step forward, extending our analysis to higher metallicities and comparing our new model predictions at solar and supersolar metallicities with the sample of Galactic PNe recently studied by Delgado-Inglada et al. (2015). The Delgado-Inglada et al. (2015) work is based on high-quality optical spectra in conjunction with the best available ionization correction factors (ICFs), which allowed an accurate determination of the nebular abundances of He, C, N, O, and Cl. It is to be noted here that: (i) their spectra are deep enough to detect weak lines [such as the O recombination lines (RLs)] and have a higher resolution (<4 Å; adequate to avoid blends) than most works in the literature (usually >7 Å); (ii) they used the most recent ICFs (Delgado-Inglada & Rodríguez 2014), which seem to work better (for most elements) than the commonly adopted Kingsburgh & Barlow (1994) ones; (iii) apart from the usual uncertainties from the line fluxes, they also considered the uncertainties associated with the ICFs; this gives larger uncertainties (as compared to the literature; e.g. Henry et al. 2010; Stanghellini & Haywood 2010; García-Hernández & Górny 2014) but their total abundances are more realistic; and (iv) their sample PNe have available space-based mid-IR spectra and can be classified depending on the dust features (e.g. C-rich or O-rich), which provide an independent proxy for the nature of the PNe progenitors. Indeed, we have recently compared the model predictions presented here[1] with the Delgado-Inglada et al. (2015) sub-sample of low-metallicity Galactic PNe with C-rich dust, obtaining a nice agreement between the models and the observational results of O self-enrichment in this type of PNe (García-Hernández et al. 2016).[2] Thus, the goals of the present paper are the detailed presentation of the new AGB model predictions for the HeCNO elements at solar/supersolar metallicity as well as their comparison with the Delgado-Inglada et al. (2015) samples of higher metallicity Galactic PNe with double- (both C- and O-rich) and O-chemistry dust in their *Spitzer Space Telescope* and/or *Infrared Space Observatory* mid-IR spectra. We describe the numerical and physical input of the AGB models as well as the evolution of the surface chemistry (focused on the CNO elements) during the AGB in Sections 2 and 3, respectively. Section 4 presents the comparison and discussion of the PN nebular abundances with the final chemical composition from the AGB evolutionary models, while our main conclusions are given in Section 5.

2 NUMERICAL AND PHYSICAL INPUT

The AGB models used in the present analysis have been computed by means of the ATON code for stellar evolution (Mazzitelli 1989). A detailed description of the numerical structure of the code is given in Ventura et al. (1998), whereas the most recent updates can be found in Ventura & D'Antona (2009).

The interested reader can find in the exhaustive reviews by Herwig (2005) and Karakas & Lattanzio (2014) a detailed discussion on the main features of the AGB evolution. The works by Ventura & D'Antona (2005a,b) and Doherty et al. (2014a,b) present a clear analysis of the uncertainties affecting the description of this evolutionary phase, in particular how the treatment of convection (both in

[1] García-Hernández et al. (2016) only gave a brief overview of the AGB ATON model predictions presented here, leaving a more detailed presentation/discussion of these models (especially the new solar/supersolar ones) to the present paper.

[2] The only nucleosynthesis models available at that time, predicting the O production in some low-mass stars, were those by Pignatari et al. (2016) (only very recently being accepted for publication).

Downloaded from https://academic.oup.com/mnras/article-abstract/461/1/542/2595305 by guest on 13 June 2020

Table 1. Chemical and evolution properties of AGB models.

Z	Y	$[\alpha/Fe]$	M_C	M_{HBB}	M_{up}
4×10^{-3}	0.25	+0.2	1.1	3.5	6.0
8×10^{-3}	0.26	+0.2	1.2	3.5	6.0
0.018	0.28	0.0	1.4	3.5	5.5
0.04	0.30	0.0	–	4.0	4.0

terms of the convective borders and the efficiency of the convection model used), mass loss and low-temperature molecular opacities reflect into the results obtained.

The models used here were calculated with the use of the following physical ingredients:

(a) *Convection.* The convective instability was modelled according to the full spectrum of turbulence (FST, hereafter) model, developed by Canuto & Mazzitelli (1991). In regions that are unstable to convection, mixing of chemical and nuclear burning are coupled by means of a diffusion-like equation, according to Cloutman & Eoll (1976). Overshoot of convective eddies into radiatively stable regions is modelled via an exponential decay of velocities from the border of the convective zones, fixed via the Schwartzschild criterion; the e-folding distance of the decay is given by ζH_p.[3] Following the calibration of the luminosity function of carbon stars in the LMC done in Ventura et al. (2014a), we use $\zeta = 0.002$ to mimic overshoot from the base of the convective envelope and from the borders of the convective shell forming at the ignition of each TP.

(b) *Mass loss.* To model mass loss, we used the recipe by Blöcker (1995) for M-stars; this description is based on hydrodynamical models of the envelope of O-rich AGBs (Bowen 1988), accounting for pulsation and the effects of radiation pressure on dust grains. Concerning carbon stars, we used the results from the Berlin group (Wachter et al. 2002, 2008), which also consider dust formation and the consequent effects of radiation pressure on carbonaceous dust particles.

(c) *Molecular opacities.* The molecular opacities in the low-temperature regime (below 10^4 K) were calculated by means of the AESOPUS tool, developed by Marigo & Aringer (2009). With this approach the opacities are suitably constructed to follow the alteration of the chemical composition of the envelope, accounting for changes in the individual abundances of C, N and O. This is crucial for the description of the C-rich phase, because the increase in the molecular opacities, occurring when the C/O ratio approaches (and overcomes) unity, favours a considerable expansion of the surface layers of the star, with the consequent enhancement of the rate at which mass loss occurs (Ventura & Marigo 2010).

In this work we use models of metallicity $Z = 4 \times 10^{-3}$, 8×10^{-3}, 0.018 and 0.04. The range of the initial mass encompass all the models evolving through the AGB, i.e. $1\,M_\odot \leq M \leq 8\,M_\odot$. The mixture of the $Z = 0.018$ and $Z = 0.04$ models is solar-scaled, whereas for the two lower metallicity ones we use an α-enhancement $[\alpha/Fe] = +0.2$; the relative fractions of the various species are taken from Grevesse & Sauval (1998). A summary of the initial chemical composition of the four sets of models is reported in Table 1.

[3] ζH_p is the e-folding distance of the exponential decay of convective velocities within regions radiatively stable. If v_0 and HP_0 are the velocity and pressure scale height at the formal border of convection, the velocity is assumed to decay within the radiative zone as $v = v_0 \times \exp[-r/(\zeta HP_0)]$ where r is the distance from the convective border.

The $Z = 4 \times 10^{-3}$ models used here are presented and discussed in Ventura et al. (2014b), whereas the evolutionary sequences of metallicity $Z = 8 \times 10^{-3}$ are extensively illustrated in Ventura et al. (2013) (for initial mass above $3\,M_\odot$) and Ventura et al. (2014a) (low-mass models of initial mass below $3\,M_\odot$). The solar and super-solar models have been calculated appositely for the present analysis and a more extensive discussion of the corresponding evolutionary sequences will be published in separate papers; e.g. the interested reader may find deeper explanations for the evolutionary sequences at solar metallicity in Di Criscienzo et al. (2016).

3 THE EVOLUTION OF THE SURFACE CHEMISTRY DURING THE AGB PHASE

3.1 A general overview

The surface chemical composition of AGB stars is altered by TDU and HBB (see e.g. Karakas & Lattanzio 2014). The former consists in the inwards penetration of the stellar mantle, occurring at the end of each TP: the surface convection reaches layers touched by He-nucleosynthesis. Mixing of nuclearly processed matter with the external regions favours the increase in the surface content of C (mainly) and O (in minor quantities). The HBB is activated at the base of the convective envelope, when the temperature in those regions exceeds ∼30 MK. The activation of this process requires core masses above $\sim 0.8\,M_\odot$. The ignition of HBB favours CN nucleosynthesis, with production of N via proton capture by C nuclei. For temperatures above ∼80 MK the whole CNO cycling is activated, which further favours N production at the expenses of C and O.

Before entering the discussion of how the efficiency of these mechanisms depends on the mass and metallicity of the stars, we stress here that the results are highly sensitive to the treatment of the convective borders (TDU, e.g. Herwig 2000) and to the efficiency of the convective model adopted (HBB, Renzini & Voli 1981; Blöcker & Schöenberner 1991). The discussion below is based on the physical ingredients used to calculate the evolutionary sequences given in Section 2.

3.2 Changes in the chemistry of AGBs: the role of mass and metallicity

The modification of the surface chemical composition during the AGB phase is determined by the relative contributions of TDU and HBB. The efficiency of the two mechanisms depends on the core mass of the star; it is thus extremely sensitive to the initial mass of the precursors. We may distinguish four cases:

(i) Stars with initial mass above $M_{up} \sim 6\,M_\odot$ experience strong HBB, with an advanced proton-capture nucleosynthesis occurring at the bottom of the convective envelope, at temperatures above 80 MK. Owing to the choice of the Blöcker (1995) description of mass loss, ignition of HBB, with the consequent rise in the luminosity (Blöcker & Schöenberner 1991), is accompanied by a considerable increase in the rate at which mass is lost, which, in turn, makes the star to experience a small number of TPs, thus limiting the effects of TDU. The chemistry of these stars is entirely determined by HBB: the overall C+N+O is preserved, N is greatly enhanced, while part of C and O are destroyed by proton fusion. Because these stars are those experiencing the most penetrating second dredge-up (SDU, Ventura 2010), their envelope is enriched in He. The threshold mass, M_{up}, depends on the metallicity of the

Downloaded from https://academic.oup.com/mnras/article-abstract/461/1/542/2595305 by guest on 13 June 2020

star, because lower Z models, for a given initial mass, evolve on bigger cores; the values of $M_{\rm up}$ are shown in Table 1.

(ii) Stars with mass in the range $M_{\rm HBB} < M < M_{\rm up}$ evolve with core mass sufficiently large (above $0.8\,{\rm M}_{\odot}$) to experience HBB. Unlike their counterparts of higher mass [see point (i) above] they also experience TDU. Indeed in the very final AGB phases, when HBB is shut down by the consumption of the external mantle, TDU becomes the only mechanism able to alter the surface chemical composition. In low-metallicity models, these late TDU episodes may convert O-rich objects into C stars. The final chemistry of these stars will be affected by both HBB and TDU. While N will be produced in all cases, C and O may be created or destroyed, according to whether the dominant mechanism is, respectively, TDU or HBB. Here we also expect some He enrichment, though in smaller quantities in comparison with the previous case. $M_{\rm HBB}$ changes with the metallicity of the star (see Table 1), because HBB is started more easily in models of lower metallicity.

(iii) Stars with mass below $M_{\rm HBB}$ do not experience any HBB, because their core mass are not sufficiently massive for the temperature at the bottom of the surface envelope to reach the minimum value (∼30 MK) required to ignite HBB. TDU is the only mechanism active in changing the surface chemical composition, thus provoking a considerable increase in the surface C and, at a smaller extent, in the O content (see e.g. García-Hernández et al. 2016). A minimum threshold mass, $M_{\rm C}$, exists, above which the stars reach the C-star stage; lower mass AGBs consume their envelope before the C/O > 1 condition is achieved. $M_{\rm C}$ is lower with decreasing Z (see Table 1), because: (a) TDU is more efficient in lower-Z models (Boothroyd & Sackmann 1988a,b); b) when the metallicity is low, the star contains a lower amount of O, thus a smaller quantity of C is needed to reach the C-star stage.

(iv) Models with initial mass below $M_{\rm C}$ never reach the C-star stage. These objects evolve as O-rich stars; their surface chemistry is altered solely by the first dredge-up (FDU), while ascending the red giant branch.

3.3 The evolution of the CNO elements

Fig. 1 shows the variation of the surface abundances of N and O in the AGB models used here. For each Z we show the tracks of stars of initial mass $M = 6$, 4 and 2 $\rm M_{\odot}$, taken as representative of the stellar groups (i), (ii) and (iii), respectively, as introduced in Section 3.2.[4] We do not show low-mass stars belonging to group (iv), because the corresponding lines would show the effects of the FDU alone, causing a mere raise in the N content. On the abscissa we report the current mass of the star: the tracks start from the value of the initial mass, and move rightwards as mass is lost, via stellar winds, from the envelope.

The chemistry of $6\,{\rm M}_{\odot}$ stars is entirely determined by HBB, with the drop of the surface O and the synthesis of N. The surface C (not shown) is severely reduced in these massive AGB models. Lower-Z models, experiencing a stronger HBB, undergo a more significant variation in the surface chemical composition. The depletion in the surface O during the whole AGB phase (see Fig. 1) amounts to $\delta\log(O) \sim -0.6$ for $Z = 4 \times 10^{-3}$, $\delta\log(O) \sim -0.4$ for $Z = 8 \times 10^{-3}$, $\delta\log(O) \sim -0.25$ for $Z = 0.018$ and $\delta\log(O) \sim -0.1$ for $Z = 0.04$. The corresponding increase in N is by a factor of ∼20 in the $Z = 4 \times 10^{-3}$ model, ∼15 in the $Z = 8 \times 10^{-3}$ case, ∼8 for $Z = 0.018$ and ∼5 for $Z = 0.04$

In $2\,{\rm M}_{\odot}$ models the change in the surface chemical composition occurs as a consequence of repeated TDU events. The rise of the surface C (by far in excess of the O enhancement) may eventually turn an O-rich object into a C star, once the C/O ratio exceeds unity. This occurs in all the $2\,{\rm M}_{\odot}$ models shown in Fig. 1, with the exception of the $Z = 0.04$ case. For these stars, not experiencing any HBB, the extent of the variation in the surface chemical composition is very sensitive to Z (for the reasons given in Section 3.2) and to the initial mass: the higher is the mass, the higher the number of TDU episodes, the larger the overall amount of C and O transported to the star's surface. Therefore, the largest increase in the surface C is found in models whose initial mass is close to $M_{\rm HBB}$: for these stars, the C enhancement factors are $50(Z = 4 \times 10^{-3})$, $20(Z = 8 \times 10^{-3})$, $5(Z = 0.018)$ and $2(Z = 0.04)$. Concerning O, the increase in the $Z = 4 \times 10^{-3}$ and $Z = 8 \times 10^{-3}$ models of mass close to $M_{\rm C}$ are, respectively, by a factor 3 and 2. No significant O increase is found in the higher-Z models. As for what concerns N, the N content of low-mass AGBs increases by $\delta\log(N) \sim 0.4$ dex (see Fig. 1), during the FDU, whereas no additional variation is expected during the AGB phase.

Stars of mass in the range $M_{\rm HBB} < M < M_{\rm up}$ [case (ii) in Section 3.2] experience both TDU and HBB. This can be clearly seen in the $4\,{\rm M}_{\odot}$ tracks in Fig. 1 (particularly in the two upper panels, corresponding to the lower metallicities), where we can distinguish three phases: (a) the initial AGB evolution, when the surface O decreases due to HBB effects; (b) an intermediate phase, during which O is destroyed by HBB in the interpulse period, whereas it is transported to the surface by TDU; (c) the final AGB phase, when HBB is switched off, thus the surface O increases as a consequence of the sole TDU effects. Nitrogen increases during the whole AGB evolution of this class of models. Note that the N increase in the envelope is larger in this case than in their higher mass counterparts because not only the C initially present in the star is used to produce N via proton-capture, but also because of the primary C dredged-up from the ashes of the He burning shell.

3.4 The final chemistry of AGBs

While the temporal evolution of the surface chemistry of AGBs allows to calculate the yields of the different elements, the interpretation of the PNe chemistry requires the surface mass fractions of the various species at the end of the AGB phase.

The final chemistry of the models used in the present analysis is shown in the four panels of Fig. 3. Besides the CNO elements and He, we also show the Cl abundance, because it is used as a good metallicity indicator by Delgado-Inglada et al. (2015). The latter element is not expected to experience any processing during the AGB phase, remaining constant during the full stellar life. The surface Cl is therefore the same as in the gas from which the star formed; thus the theoretical predictions depend on the choice of the initial mixture. The plots in Fig. 3 were obtained based on the solar and α-enhanced mixture given by Grevesse & Sauval (1998). We note, however, that the He abundance and the abundance ratios used here (e.g. N/O, N/Cl, C/O) are consistent with similar models calculated with the more recent Asplund et al. (2009) solar abundances; this is also the case for the Monash AGB models (Karakas, private communication). The massive AGB models eventually tend to the HBB equilibrium values, which are primarily determined by the temperature at the base of the convective zone, with scarce effect

[4] Because the C-star stage is never reached in the Z=0.04 case, the $M = 2\,{\rm M}_{\odot}$ model shown in the right, bottom panel of Fig. 1 is in fact representative of stars belonging to group (iv).

Downloaded from https://academic.oup.com/mnras/article-abstract/461/1/542/2595305 by guest on 13 June 2020

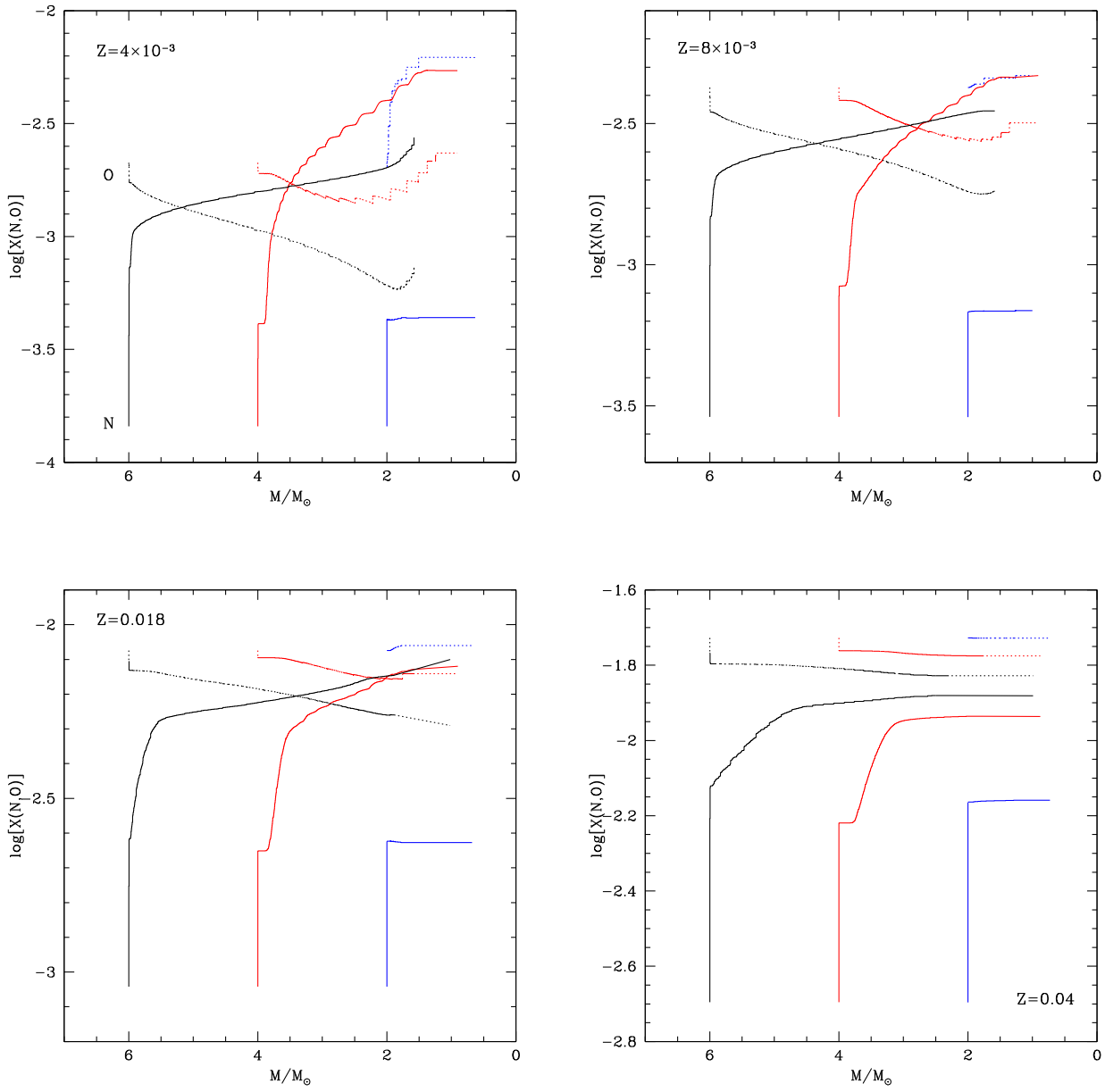


Figure 1. The variation during the AGB phase of the surface mass fraction of N (solid tracks) and O (dotted) in models of initial mass 2 (blue), 4 (red) and 6 $M_\odot$ (black) and metallicity $Z = 4 \times 10^{-3}$ (left, upper panel), 8×10^{-3} (right, upper panel), 0.018 (left, lower panel) and 0.04 (right, lower panel). The vertical scale is logarithmic, to allow a better coverage of the whole range of N and O abundances involved. On the abscissa we report the current mass of the star.

of the initial chemical composition. This holds in particular for the CNO elements, which are fully involved in the nuclear activity at the base of the envelope. For the less massive AGB stars, reaching the C-star stage, what matters is the amount of C and O dredged-up to the stellar surface. The latter is largely determined by the increase in the mass-loss rate that occurs after becoming a C-star, while the initial chemistry is completely forgotten.

The top panels of Fig. 3 show the final abundances of N and O. The range of N and O is more extended in models of lower metallicity because, as outlined in Section 3.2, both HBB and TDU are more efficient in lower-Z environments.

The range of C/O values covered by the models is similar for the four metallicities, while the range of the individual C and O abundances is extremely sensitive to Z; the differences cancel when the C/O ratio is computed. The largest C/O (over a factor of 10 higher than in the initial mixture) is found in the $Z = 4 \times 10^{-3}$ models, for the same arguments given in Section 3.2.

The distribution of the chemical composition in the N/O versus He plane (right-bottom panel of Fig. 3) is less straightforward. Generally speaking, N/O is an indicator of the strength of HBB, while He is related to the inwards penetration of the convective envelope during the SDU. The efficiency of the latter mechanism, provoking the increase in the surface He, increases with the mass of the star (Ventura 2010). The distribution of the models in this plane is dychotomic. Low mass AGB stars trace an approximately vertical sequence, with constant He – no SDU is expected below ∼4 $M_\odot$

Downloaded from https://academic.oup.com/mnras/article-abstract/461/1/542/2595305 by guest on 13 June 2020

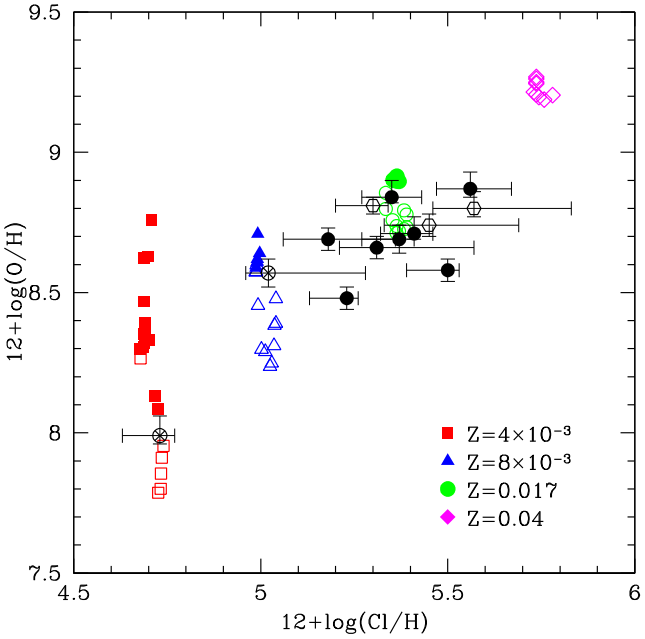


Figure 2. The distribution of the Cl abundances versus the O ones in the double-chemistry (DC) and oxygen-chemistry (OC) PNe by Delgado-Inglada et al. (2015) and of the final abundances of the AGB models at several metallicities. The DC and OC PNe are shown with solid and open-crossed circles, respectively, while the three OC PNe (M 2-42, NGC 3132 and NGC 6543) with more uncertain dust classifications (see the text for more details) are shown with open hexagons. Full (open) model points indicate carbon(oxygen)-rich chemistry.

and variable (though always below ∼0.3) N/O. Higher mass AGB models, experiencing HBB are, however, spread on the right, upper region of the N/O–He plane.

4 UNDERSTANDING THE GALACTIC PNE SAMPLE WITH PRECISE NEBULAR ABUNDANCES

The Delgado-Inglada et al. (2015) sub-sample (seven objects) of lower metallicity Galactic PNe with C-dust features in their mid-IR spectra has been recently analysed by us (García-Hernández et al. 2016). We note that, on average, the Galactic PNe with C-rich dust features (in the form of aliphatic hydrocarbons), not analysed here, are of lower metallicity than the double- and O-dust PNe. By comparing the observed chemistry (HeCNOCl) with the ATON AGB models detailed here, García-Hernández et al. (2016) concluded that they mostly descend from low-metallicity ($Z = 8 \times 10^{-3}$) low-mass (∼1−3 $M_{\odot}$) AGB stars that produce O, confirming that O is not always a good metallicity indicator (especially in low-metallicity C-rich dust PNe). In the present sample of OC and DC PNe (see below) the situation is different (significant O production/destruction is, in principle, not expected; Delgado-Inglada et al. 2015, see also Fig. 2) and O is a more reliable metallicity indicator. This is shown in Fig. 2, which displays the Cl/H and O/H abundances; Fig. 2, however, is not the most useful to distinguish the PNe progenitors (see Fig. 3 for additional abundance ratios).

The observed chemistry of the Delgado-Inglada et al. (2015) remaining sample (13 objects) of Galactic PNe span a wide range of metallicities (by more than one order of magnitude) as suggested by the Cl content (see below), which is taken as a metallicity indicator.[5] By following the García-Hernández & Górny (2014) dust type/subtype nomenclature, the available *ISO* and/or *Spitzer* mid-IR spectra (Delgado-Inglada & Rodríguez 2014, see e.g. their table 6) are classified into two major dust types (oxygen chemistry or OC and double chemistry or DC) and subtypes – amorphous (*am*) and crystalline (*cr*) – depending on the nature of the dust features; O-rich (OC) or both C- and O-rich (DC). Eight out of the thirteen sources in the sample are surrounded by both C-rich and O-rich dust, in the form of polycyclic aromatic hydrocarbon (PAH) features and amorphous and/or crystalline silicates, respectively. Five sources only display traces of amorphous (*am*) and/or crystalline (*cr*) silicate features (O-rich dust) in their IR spectra. Table 2 lists our Galactic PNe sample together with their IR dust types/subtypes as well as the main abundance ratios used in this work.

The DC-type PNe display Cl abundances from subsolar (12+log(Cl/H)∼5.2) to slightly supersolar (12+log(Cl/H)∼5.6), while the OC-type ones span an even larger Cl range, from very low-metallicity (12+log(Cl/H)∼4.7; PN DdDm 1) to supersolar values (12+log(Cl/H)∼5.6; PN NGC 6543). Fig. 3 shows the chemical composition of our present Galactic PNe sample in comparison with the AGB model predictions; for comparison we also show the median He and N/O values of Galactic OC and DC PNe as measured by García-Hernández & Górny (2014) from low-resolution optical spectra and using the Kingsburgh & Barlow (1994) ICFs.[6] Unlike the C-rich dust PNe (García-Hernández et al. 2016), here the errors associated with the individual abundances (especially for the C/O ratio), the higher spread in metallicity, and uncertainties in the dust type/subtype for some objects (see below) do not allow a straight determination of the AGB progenitor mass and the formation epoch of the DC and OC PNe samples. In any case, some interesting conclusions may be extracted from the models versus observations comparison, although it should be more focused on a star-by-star basis.

As we mentioned above, the O-dust chemistry PNe are generally more metal-rich than their C-dust chemistry counterparts (Delgado-Inglada et al. 2015; García-Hernández et al. 2016). The only exceptions are the halo PN DdDm 1 and NGC 6210,[7] which show a much smaller and a similar metallicity, respectively; DdDm 1 is also the only OC PN showing amorphous silicates in emission (OC_{am} in Table 2). Both objects have a small N content, pointing against HBB contamination; this is also confirmed by their low N/O ratios and He abundances. Their chemistries are consistent with low-mass (∼1 $M_{\odot}$), low-metallicity ($Z = 4 - 8 \times 10^{-3}$) progenitors, formed ∼ 5–6 Gyr ago,[8] that did not reach the C-star stage [group (iv) in Section 3.2]. Our interpretation for PN DdDm 1, based on the ATON AGB models, is fully consistent with the results from *Spitzer* mid-IR spectroscopy of Galactic PNe (Stanghellini et al. 2012) and their correlation with the chemical abundances from low-resolution optical spectra (basically He and the N/O ratio; García-Hernández & Górny 2014, see Fig. 3), which show that Galactic OC_{am} PNe

[5] For consistency with the ATON AGB models, we consider the solar Cl abundance of 12+log(Cl/H) = 5.50 (Grevesse & Sauval 1998).
[6] García-Hernández & Górny (2014) only could measured the Cl abundances in a few PNe and they are very uncertain.
[7] Based on the observed morphology, Soker (2016) very recently speculates that this PN could be the result of triple-stellar evolution with a tight binary system.
[8] The formation epoch estimates are according to ATON and are model dependent. In particular the ATON evolutionary time-scales are usually shorter than other AGB models in the literature such as those by Karakas (2010) (see also fig. 1 in García-Hernández et al. 2013).

Downloaded from https://academic.oup.com/mnras/article-abstract/461/1/542/2595305 by guest on 13 June 2020

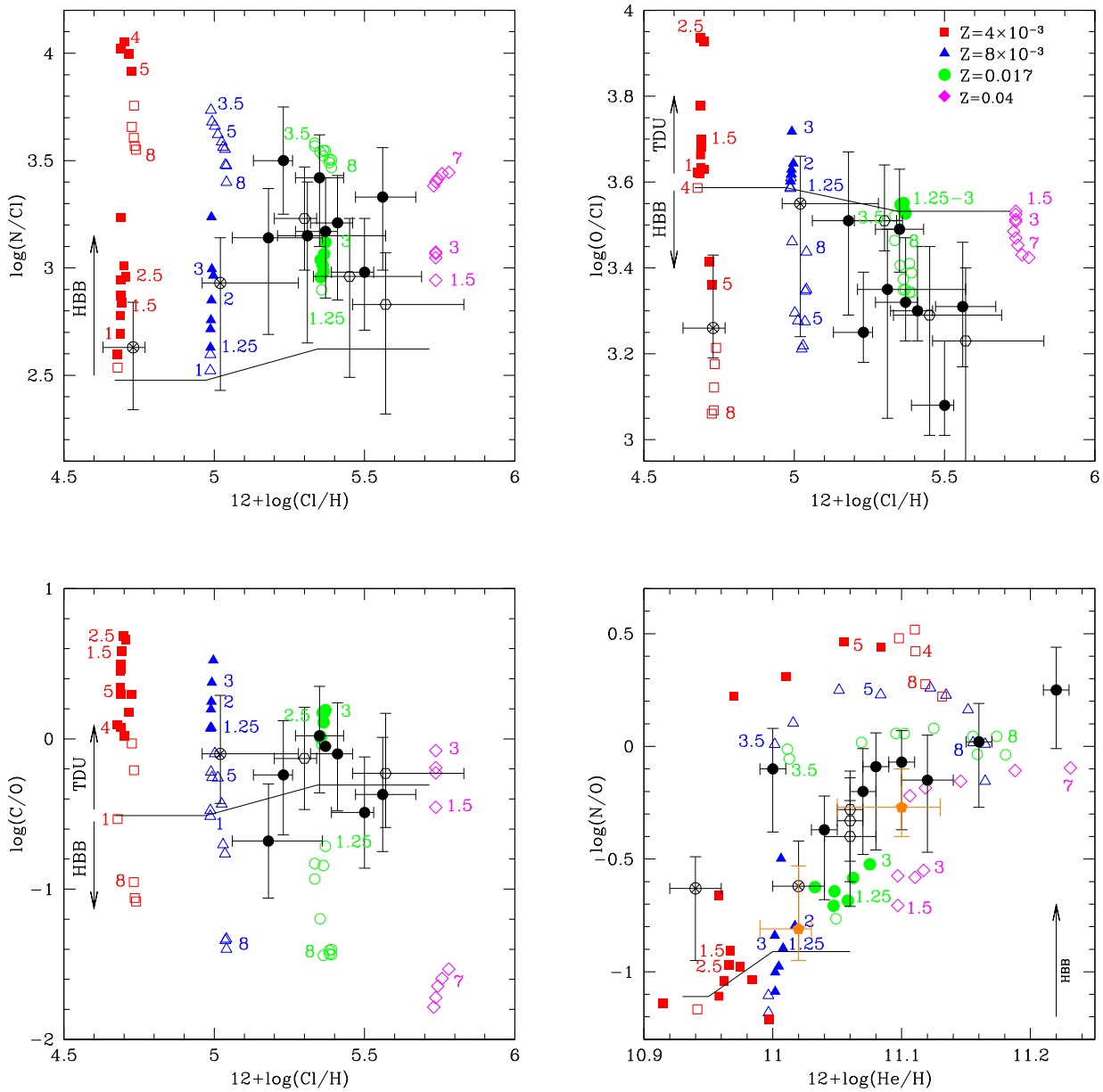


Figure 3. The distribution of the chemistry of the double chemistry (DC) and oxygen-chemistry (OC) PNe by Delgado-Inglada et al. (2015) and of the final mass fractions of the AGB models of various metallicities in the Cl versus N/Cl (top, left panel), Cl versus O/Cl (top, right), Cl versus C/O (bottom, left) and He versus N/O (bottom, right) planes. The DC and OC PNe are shown with solid and open-crossed circles, respectively, while the three OC PNe (M 2-42, NGC 3132 and NGC 6543) with more uncertain dust classifications (see the text for more details) are shown with open hexagons. Full (open) model points indicate carbon(oxygen)-rich chemistry. The thin, solid lines indicate the assumed initial abundances in the models. The arrows indicate the qualitative effect of HBB and of the SDU and TDU. The orange pentagons (bottom-right panel) are the median abundances (and their observed range as 25 and 75 percentiles) of Galactic OC (at 12+log(He/H)≃11.02) and DC (at 12+log(He/H)≃11.1) PNe measured by García-Hernández & Górny (2014).

display higher Galactic latitudes than the OC_{cr} ones and their He and N/O ratios are consistent with their progenitors being the lowest metallicity and lowest mass AGB stars in our Galaxy, respectively.[9]

The other three O-rich dust PNe (M 2-42, NGC 3132 and NGC 6543) display higher metallicities, between slightly subsolar and supersolar. We note, however, that the dust classes for the OC PNe M 2-42 and NGC 3132 (both classified as OC_{cr}, Table 2) and NGC 6543 (classified as OC_{am+cr}, Table 2) are more uncertain. M 2-42 displays the lowest S/N IR spectrum in our sample and only low-resolution (R∼100) spectra are available, while NGC 3132 displays a rather noisy IR spectrum, which looks different to the rest of IR spectra (especially the slope of the underlying IR dust continuum emission between 10 and 38 μm). Both objects display a weak PAH-like feature at 11.3 μm that seems to be not accompanied by the other PAH-like features at ∼6.2, 7.7, and 8.6 μm (Delgado-Inglada & Rodríguez 2014). On the other hand, NGC 6543 only has a rather noisy *ISO* (much less sensitive than *Spitzer*) spectrum available

[9] A similar comparison for NGC 6210 is not possible because such low-metallicity OC_{cr} objects are absent in the García-Hernández & Górny (2014) sample of PNe with *Spitzer* spectra.

Downloaded from https://academic.oup.com/mnras/article-abstract/461/1/542/2595305 by guest on 13 June 2020

Table 2. Main abundance ratios[a] and IR dust types/subtypes in our Galactic PNe sample.

Object	12+log(Cl/H)	12+log(O/H)	log(N/Cl)	log(O/Cl)	log(C/O)	log(N/O)	12+log(He/H)	Dust type[b]	Source[c]
				DC PNe					
Cn 1-5	5.35±0.08	$8.84^{+0.06}_{-0.02}$	$3.42^{+0.20}_{-0.32}$	$3.49^{+0.14}_{-0.10}$	$0.02^{+0.33}_{-0.38}$	$-0.07^{+0.18}_{-0.26}$	11.10±0.01	DC_{cr}	*ISO*/*Spitzer*
H 1-50	$5.18^{+0.18}_{-0.12}$	8.69±0.04	$3.14^{+0.29}_{-0.39}$	$3.51^{+0.22}_{-0.16}$	−0.68±0.38	$-0.37^{+0.15}_{-0.31}$	11.04±0.01	DC_{am+cr}?	*Spitzer*
M 1-42	$5.23^{+0.03}_{-0.10}$	8.48±0.04	$3.50^{+0.18}_{-0.32}$	$3.25^{+0.07}_{-0.14}$	$-0.24^{+0.36}_{-0.40}$	$0.25^{+0.19}_{-0.26}$	11.22±0.01	DC_{cr}	*ISO*/*Spitzer*
M 2-27	$5.56^{+0.11}_{-0.09}$	$8.87^{+0.06}_{-0.03}$	$3.33^{+0.25}_{-0.32}$	$3.31^{+0.17}_{-0.12}$	−0.37±0.38	$0.02^{+0.20}_{-0.26}$	11.16±0.01	DC_{cr}	*Spitzer*
M 2-31	$5.31^{+0.26}_{-0.10}$	8.66±0.04	$3.15^{+0.41}_{-0.34}$	$3.35^{+0.30}_{-0.14}$	–	$-0.20^{+0.19}_{-0.28}$	11.07±0.01	DC_{cr}	*Spitzer*
MyCn 18	$5.50^{+0.03}_{-0.11}$	8.58±0.04	$2.98^{+0.17}_{-0.35}$	$3.08^{+0.07}_{-0.15}$	−0.49±0.37	$-0.10^{+0.18}_{-0.28}$	11.00±0.01	DC_{am+cr}	*Spitzer*
NGC 6439	$5.37^{+0.04}_{-0.10}$	8.69±0.05	$3.17^{+0.19}_{-0.37}$	$3.32^{+0.09}_{-0.15}$	$-0.05^{+0.37}_{-0.41}$	$-0.15^{+0.20}_{-0.32}$	11.12±0.02	DC_{cr}	*Spitzer*
NGC 7026	$5.41^{+0.05}_{-0.09}$	$8.71^{+0.06}_{-0.02}$	$3.21^{+0.18}_{-0.40}$	$3.30^{+0.11}_{-0.11}$	$-0.10^{+0.34}_{-0.38}$	$-0.09^{+0.19}_{-0.33}$	11.08±0.01	DC_{cr}	*Spitzer*
				OC PNe					
DdDm 1	$4.73^{+0.04}_{-0.10}$	$7.99^{+0.07}_{-0.03}$	$2.63^{+0.15}_{-0.35}$	$3.26^{+0.11}_{-0.13}$	–	$-0.63^{+0.18}_{-0.28}$	10.94±0.02	OC_{am}	*Spitzer*
M 2-42	$5.45^{+0.24}_{-0.12}$	8.74±0.04	$2.96^{+0.39}_{-0.35}$	$3.29^{+0.28}_{-0.16}$	–	$-0.33^{+0.19}_{-0.27}$	11.06±0.01	OC_{cr}?	*Spitzer*
NGC 3132	$5.30^{+0.04}_{-0.10}$	8.81±0.03	$3.23^{+0.18}_{-0.30}$	$3.51^{+0.07}_{-0.13}$	−0.13±0.34	$-0.28^{+0.17}_{-0.23}$	11.06±0.01	OC_{cr}?	*Spitzer*
NGC 6210	$5.02^{+0.26}_{-0.06}$	8.57±0.05	$2.93^{+0.41}_{-0.30}$	$3.55^{+0.31}_{-0.11}$	$-0.10^{+0.39}_{-0.33}$	$-0.62^{+0.20}_{-0.29}$	11.02±0.02	OC_{cr}	Spitzer
NGC 6543	$5.57^{+0.26}_{-0.11}$	$8.80^{+0.06}_{-0.03}$	$2.83^{+0.39}_{-0.36}$	$3.23^{+0.32}_{-0.14}$	$-0.23^{+0.40}_{-0.36}$	$-0.40^{+0.19}_{-0.28}$	11.06±0.02	OC_{am+cr}?	*ISO*

Notes. [a]Abundance ratios and uncertainties from Delgado-Inglada et al. (2015).
[b]IR dust type/subtype from Delgado-Inglada & Rodríguez (2014) but following the nomenclature by García-Hernández & Górny (2014). Questions marks indicate a rather uncertain dust classification (see the text for more details).
[c]The available *ISO* and/or *Spitzer* mid-IR spectra can be consulted in Delgado-Inglada & Rodríguez (2014) (see also references in their Table 6).

(Bernard-Salas & Tielens 2005), which hampers the detection of any dust feature in the PAHs spectral region. This together with their nearly solar Cl abundances of 12+log(Cl/H)=5.30 (NGC 3132), 5.45 (M 2-42) and 5.57 (NGC 6543) indicate that these PNe could be truly DC PNe where the PAH-like features may have escaped detection by *Spitzer* and *ISO*; note that NGC 3132 is also suspected to have a binary companion (e.g. Sahu & Desai 1986). García-Hernández & Górny (2014) also found a few similar examples of Galactic OC PNe with crystalline silicates (e.g. OC_{cr}) showing a chemical nebular gas pattern (e.g. He, Ar, and N/O) identical to the one of DC PNe. Their possible link with DC PNe is also suggested by our Fig. 3 where the three objects (marked with open diamonds) are indistinguishable from the rest of DC PNe in our sample.

The double-dust chemistry PNe are also more metal-rich than the C-dust chemistry ones (Delgado-Inglada et al. 2015; García-Hernández et al. 2016) and, on average, even more metal-rich (12+log(Cl/H) $\geq$ 5.2) than the OC-type PNe (Fig. 3). Six out of the eight DC sources only display crystalline silicates (DC_{cr}-type in Table 2). The only exceptions are MyCn 18 and H 1-50, which are classified as DC_{am+cr} PN because they also displays amorphous silicates in emission; although the amorphous silicates emission in H 1-50 is very weak. It is to be noted here that although Cn 1-5 and H 1-50 pertain to the DC class, they show *Spitzer* spectra that are clearly different from the rest of DC PNe, which show the typical DC spectrum with weak PAH-like bands and crystalline/amorphous silicates. The Cn 1-5 IR spectrum display very strong PAH-like features and unidentified 24 μm emission; curiously, this is the only DC object in our sample with C/O $\geq$ 1 (but also consistent, within the errors, with C/O < 1). The Cn 1-5 C/O ratio is higher than one using both RLs and collisionally excited lines (CELs) (Delgado-Inglada & Rodríguez 2014), suggesting a true C-rich gas nebula. The H 1-50 IR spectrum, however, shows tentative PAH-like features and the general shape of the IR spectrum is quite similar to other OC PNe such as NGC 6210 or even DdDm 1. The PN H 1-50 may thus be a truly OC object. Indeed, H 1-50 displays the lowest He and N/O ratios in the DC group, suggesting a less massive progenitor than other objects of similar metallicity such as M 2-42. Again, the individual abundances errors (especially for the key C/O ratio) and the spread in metallicity difficult the determination of the AGB progenitor masses of the DC PNe as a whole; exceptions to this limitation are PNe M 1-42 and M 2-27 (see below). The DC PNe almost cover all possible initial masses in the Cl versus N/Cl, Cl versus O/Cl and Cl versus C/O planes (Fig. 3). However, the He versus N/O plane (bottom, right-hand panel in Fig. 3) suggests that, according to the ATON AGB models, DC PNe are mostly the descendants of the higher mass (M $\geq$3.5 $M_{\odot}$) AGB progenitors, experiencing HBB, at solar/supersolar metallicity (formed ∼50–250 Myr ago). This is consistent with Delgado-Inglada et al. (2015), who compared with other AGB nucleosynthesis predictions in the literature (e.g. those from Karakas 2010)[10] and García-Hernández & Górny (2014) where the median He and N/O abundances (from low-resolution optical spectroscopy; see Fig. 3) of larger samples of Galactic disc and bulge DC PNe were found to be consistent with the Karakas (2010) predictions for ∼5 $M_{\odot}$ solar metallicity HBB AGB stars.[11] However, as already pointed out by García-Hernández & Górny (2014) and Delgado-Inglada et al. (2015), less massive (<3.5 $M_{\odot}$) non-HBB stars could also produce the high He and N/O ratios observed in DC PNe via extra mixing, stellar rotation, binary interaction, or even He pre-enrichment.

Interestingly, MyCn 18 and M 1-42 (and M 2-27) seem to be examples of objects at the lower and higher end, respectively, of the AGB progenitor masses covered by DC PNe in the He versus N/O plane. The PN MyCn 18 seems to be the descendant of a solar metallicity ∼3.5 $M_{\odot}$ AGB progenitor, formed ∼250 Myr ago. The chemical composition of PNe M 1-42 and M 2-27, however,

[10] Delgado-Inglada et al. (2015) also used the model predictions by Pignatari et al. (2016), although not accepted at that time.
[11] The minimum mass to activate HBB is model dependent; e.g. at solar metallicity it is ∼3.5 $M_{\odot}$ in our ATON AGB models, while it is ∼4.5 $M_{\odot}$ in the Karakas (2010) ones.

Downloaded from https://academic.oup.com/mnras/article-abstract/461/1/542/2595305 by guest on 13 June 2020

clearly reflects the effects of HBB, because they are enriched in N and have an O content significantly smaller than the average value of other sample PNe at similar metallicities. Furthermore, they are the two PNe with the highest He abundances, suggesting that they descend from stars of mass $\sim 6 - 7\,M_{\odot}$ and metallicity slightly subsolar (M 1-42) and supersolar (M 2-27). The evolutionary times of AGB stars of this mass and metallicity indicate a relatively recent formation epoch, between 40 and 80 Myr ago. According to our modelling, these stars should belong to group (i) in Section 3.2, thus their chemical composition should show-up the imprinting of HBB, with no signatures of TDU. However, the recommended C/O ratios are at odds with this hypothesis, as they are a factor $\sim$5 higher than predicted (see left, bottom panel of Fig. 3), suggesting some contribution from TDU. This possibility was advanced by García-Hernández et al. (2006, 2007, 2013), to explain the Rb overabundances observed in massive Galactic AGB stars, undergoing HBB.

Still in the context of massive AGBs, Ventura et al. (2015) outlined that some of the PNe in the LMC can be interpreted as the progeny of 6–7 $M_{\odot}$ stars, whose surface chemistry was contaminated exclusively by HBB. Clearly the comparison among the two samples is not straightforward, because the metallicities of the PNe are different. However, confirmation of the C/O values provided by Delgado-Inglada et al. (2015) would suggest larger effects from TDU in solar/supersolar metallicity massive AGB stars. In the context of our modelling, larger TDU effects would indicate that the mass-loss rate in our massive AGB models of solar and supersolar metallicity is too high. Alternatively, the true C/O ratios of M 1-42 and M 2-27 could be smaller than the Delgado-Inglada et al. (2015) recommended values,[12] thus rendering the agreement with the models more satisfactory.

In short, the comparison with the ATON models suggests that: (i) the lowest metallicity OC PNe should be the descendants of low-mass ($\sim$1 $M_{\odot}$) stars that are not converted into C-rich stars, while the higher metallicity OC ones (with uncertain dust classifications and DC-like chemical compositions) could be truly DC PNe where the PAH-like features may have escaped detection in the available mid-IR space-based spectroscopic observations; (ii) solar/supersolar metallicity DC PNe should be the descendants of the higher mass (M $\geq$3.5 $M_{\odot}$) HBB AGB stars but alternative channels of formation cannot be discarded with the present nebular abundances and their associated errors.

5 CONCLUSIONS

We use AGB models (with diffusive overshooting from all the convective borders) of different metallicity (from $Z_{\odot}/4$ to $2Z_{\odot}$) to interpret the surface chemistry (He, C, N, O, and Cl) of a sample of Galactic PNe with high-quality spectra, which together with the best ICFs available allowed abundance determinations with unprecedented accuracy/reliability (Delgado-Inglada et al. 2015). The PNe investigated are divided among double-dust chemistry (DC) and oxygen-dust chemistry (OC) according to the dust features present in their available space-based IR spectra.

Unlike the Delgado-Inglada et al. (2015) subsample of carbon-dust chemistry (CC) PNe recently analysed by us (García-Hernández et al. 2016), here the individual abundance errors (in particular for the C/O ratio), the wider metallicity range, and the uncertain dust types/subtypes in some objects do not permit a clear determination of the AGB initial mass (and the formation epoch) for both PNe samples. The PNe observations versus AGB models comparison is thus more focused on a star-by-star basis.

The two lowest metallicity OC PNe (DdDm 1 and NGC 6210) are interpreted as the descendants of low-mass ($\sim$1 $M_{\odot}$) AGB stars that did not reach the C-rich phase. The three higher metallicity PNe in this group (M 2-42, NGC 3132 and NGC 6543) have uncertain dust classifications and are chemically indistinguishable from the rest of DC PNe in our sample, being interpreted as truly DC PNe where the PAH-like features may have escaped detection by the *Spitzer* and *ISO* satellites.

The DC PNe in our Galaxy may display different kind of IR spectra and, sometimes, even C/O ratios over unity (e.g. Cn 1-5). However, we still lack complete samples of Galactic DC PNe with precise C/O ratios. We find that the DC PNe in our sample are best separated (in terms of progenitor AGB masses) in the He versus N/O plane, which otherwise suggests that they mostly descend from the higher mass (M $\geq$3.5 $M_{\odot}$) HBB AGB stars at solar/supersolar metallicity. This is consistent with recent works in the literature, and also we cannot discard alternative formation channels in low-mass non-HBB stars such as extra mixing, stellar rotation, binary interaction, or He pre-enrichment. More precise C/O ratios turn out to be fundamental to learn about the stellar origin of DC PNe.

The DC PN MyCn 18 seems to be at the lower end ($\sim$3.5 $M_{\odot}$) of the AGB progenitor masses covered by the DC PNe in our sample. On the other hand, two DC PNe (M 1-42 and M 2-27) are likely descendants of the more massive AGB stars of close-to-solar chemistry, with mass $\sim 6 - 7\,M_{\odot}$, formed 40–80 Myr ago. This is deduced on the basis of the large content of N and He, and the low O. The recommended C/O ratio of these two objects (C/O $\sim$ 0.5), if confirmed, suggests a role by TDU in the contamination of the surface chemistry during the previous AGB phase. This is at odds with our AGB model predictions, giving a significantly smaller C/O $\sim$ 0.1, with only a modest contamination from TDU. Also, confirmation of this finding would indicate an intrinsic difference among the evolution of massive AGBs, likely progenitors of the DC PNe studied here, and their lower metallicity counterparts in the Magellanic Clouds, which, as shown by Ventura et al. (2015, 2016), are contaminated by HBB only. A more robust determination of the C/O ratio of these two particular PNe is a promising opportunity to assess any possible contribution of TDU in altering the surface chemical composition of massive AGB stars in solar and supersolar environments.

ACKNOWLEDGEMENTS

DAGH was funded by the Ramón y Cajal fellowship number RYC−2013−14182 and he acknowledges support provided by the Spanish Ministry of Economy and Competitiveness (MINECO) under grant AYA−2014−58082-P. PV was supported by PRIN MIUR 2011 'The Chemical and Dynamical Evolution of the Milky Way and Local Group Galaxies' (PI: F. Matteucci), prot. 2010LY5N2T. GDI acknowledges support from the Mexican CONACYT grant CB−2014−241732. FDA acknowledges support from the Observatory of Rome.

[12] Delgado-Inglada & Rodríguez (2014) obtained a C/O ratio of 0.36 (from CELs) and 0.56 (from RLs) and of only 0.32 (from RLs) for M 1-42 and M 2-27, respectively, suggesting also that these abundance ratios are uncertain and better spectra and calculations would be needed.

Downloaded from https://academic.oup.com/mnras/article-abstract/461/1/542/2595305 by guest on 13 June 2020

REFERENCES

Asplund M., Grevesse N., Sauval A. J., Scott P., 2009, ARA&A, 47, 481
Bernard-Salas J., Tielens A. G. G. M., 2005, A&A, 523, 538
Blöcker T., 1995, A&A, 297, 727
Blöcker T., Schöenberner D., 1991, A&A, 244, L43
Boothroyd A. I., Sackmann I.-J., 1988a, ApJ, 328, 653
Boothroyd A. I., Sackmann I.-J., 1988b, ApJ, 328, 671
Bowen G. H., 1988, ApJ, 329, 299
Canuto V. M. C., Mazzitelli I., 1991, ApJ, 370, 295
Cloutman L. D., Eoll J. G., 1976, ApJ, 206, 54
D'Ercole A., Vesperini E., D'Antona F., McMillan S. L. W., Recchi S., 2008, MNRAS, 391, 825
Delgado-Inglada G., Rodríguez M., 2014, ApJ, 784, 173
Delgado-Inglada G., Rodriguez M., Peimbert M., Stasinska G., Morisset C., 2015, MNRAS, 449, 1797
Dell'Agli F., Ventura P., García-Hernández D. A., Schneider R., Di Criscienzo M., Brocato E., D'Antona F., Rossi C., 2014, MNRAS, 442, L38
Dell'Agli F., Ventura P., Schneider R., Di Criscienzo M., García-Hernández D. A., Rossi C., Brocato E., 2015a, MNRAS, 447, 2992
Dell'Agli F., García-Hernández D. A., Ventura P., Schneider R., Di Criscienzo M., Rossi C., 2015b, MNRAS, 454, 4235
Di Criscienzo M. et al., 2013, MNRAS, 433, 313
Di Criscienzo M., Ventura P., García-Hernández D. A., Dell'Agli F., Castellani M., Marrese P., Marinoni S., Zamora O., 2016, MNRAS, submitted
Doherty C. L., Gil-Pons P., Lau H. H. B., Lattanzio J. C., Siess L., 2014a, MNRAS, 437, 195
Doherty C. L., Gil-Pons P., Lau H. H. B., Lattanzio J. C., Siess L., Campbell S. W., 2014b, MNRAS, 441, 582
Ferrarotti A. D., Gail H. P., 2006, A&A, 553, 576
García-Hernández D. A., Górny S. K., 2014, A&A, 567, A12
García-Hernández D. A., García-Lario P., Plez B., D'Antona F., Manchado A., Trigo-Rodrííguez J. M., 2006, Science, 314, 1751
García-Hernández D. A., García-Lario P., Plez B., Manchado A., D'Antona F., Lub J., Habing H., 2007, A&A, 462, 711
García-Hernández D. A. et al., 2009, ApJ, 705, L31
García-Hernández D. A., Zamora O., Yagüe A., Uttenthaler S., Karakas A. I., Lugaro M., Ventura P., Lambert D. L, 2013, A&A, 555, L3
García-Hernández D. A., Ventura P., Delgado-Inglada G., Dell'Agli F., Di Criscienzo M., Yagüe A., 2016, MNRAS, 458, L118
Grevesse N., Sauval A. J., 1998, Space Sci. Rev., 85, 161
Henry R. B. C., Kwitter K. B., Jaskot A. E., Balick B., Morrison M. A., Milingo J. B., 2010, ApJ, 724, 748
Herwig F., 2000, A&A, 360, 952
Herwig F., 2005, ARA&A, 43, 435
Karakas A. I., 2010, MNRAS, 403, 1413
Karakas A. I., Lattanzio J. C., 2014, Publ. Astron. Soc. Aust., 31, 30
Kingsburgh R. L., Barlow M. J., 1994, MNRAS, 271, 257
Maraston C., Daddi E., Renzini A., Cimatti A., Dickinson M., Papovich C., Pasquali A., Pirzkal N., 2006, ApJ, 652, 85
Marigo P., Aringer B., 2009, A&A, 508, 1538
Marigo P., Bernard-Salas J., Pottasch S. R., Tielens A. G. G. M., Wesselius P. R., 2003, A&A, 409, 619
Marigo P., Bressan A., Girardi L., Aringer B., Gullieuszik M., Groenewegen M. A. T., 2011, in Kerschbaum F., Lebzelter T., Wing R. F., eds, ASP Conf. Ser. Vol. 445, Why Galaxies Care about AGB Stars II: Shining Examples and Common Inhabitants. Astron. Soc. Pac., San Francisco, p. 431
Mazzitelli I., 1989, ApJ, 340, 249
Mazzitelli I., D'Antona F., Ventura P., 1999, 348, 846
Nanni A., Bressan A., Marigo P., Girardi L., 2013a, MNRAS, 434, 488
Nanni A., Bressan A., Marigo P., Girardi L., 2013b, MNRAS, 434, 2390
Nanni A., Bressan A., Marigo P., Girardi L., 2014, MNRAS, 438, 2328
Pignatari M. et al., 2016, ApJS, preprint (arXiv:1307.6961)
Renzini A., Voli M., 1981, A&A, 94, 175
Romano D., Karakas A. I., Tosi M., Matteucci F., 2010, A&A, 522, A32
Sahu K. C., Desai J. N., 1986, A&A, 161, 357
Santini P. et al., 2014, A&A, 562, A30
Schwarzschild M., Harm R., 1965, ApJ, 142, 855
Schwarzschild M., Harm R., 1967, ApJ, 150, 961
Soker N., 2016, MNRAS, 455, 1584
Stanghellini L., Haywood M., 2010, ApJ, 714, 1096
Stanghellini L., Lee T.-H., Shaw R. A., Balick B., Villaver E., 2009, ApJ, 702, 733
Stanghellini L., García-Hernández D. A., García-Lario P., Davies J. E., Shaw R. A., Villaver E., Manchado A., Perea-Calderóón J. V., 2012, ApJ, 753, 172
Valiante R., Schneider R., Salvadori S., Bianchi S., 2011, MNRAS, 416, 1916
Ventura P., 2010, in Charbonnel C., Tosi M., Primas F., Chiappini C., eds, Proc. IAU Symp. 268, Light Elements in the Universe. Kluwer, Dordrecht, p. 147
Ventura P., D'Antona F., 2005a, A&A, 431, 279
Ventura P., D'Antona F., 2005b, A&A, 439, 1075
Ventura P., D'Antona F., 2009, MNRAS, 499, 835
Ventura P., Marigo P., 2010, MNRAS, 408, 2476
Ventura P., Zeppieri A., Mazzitelli I., D'Antona F., 1998, A&A, 334, 953
Ventura P., D'Antona F., Mazzitelli I., Gratton R., 2001, ApJ, 550, L65
Ventura P. et al., 2012a, MNRAS, 420, 1442
Ventura P. et al., 2012b, MNRAS, 424, 2345
Ventura P., Di Criscienzo M., Carini R., D'Antona F., 2013, MNRAS, 431, 3642
Ventura P., Dell'Agli F., Di Criscienzo M., Schneider R., Rossi C., La Franca F., Gallerani S., Valiante R., 2014a, MNRAS, 439, 977
Ventura P., Di Criscienzo M. D., D'Antona F., Vesperini E., Tailo M., Dell'Agli F., D'Ercole A, 2014b, MNRAS, 437, 3274
Ventura P., Stanghellini L., Dell'Agli F., García-Hernández D. A., Di Criscienzo M., 2015, MNRAS, 452, 3679
Ventura P., Stanghellini L., Di Criscienzo M., García-Hernández D. A., Dell'Agli F., 2016, MNRAS, preprint (arXiv:1605.09300)
Wachter A., Schröder K. P., Winters J. M., Arndt T. U., Sedlmayr E., 2002, A&A, 384, 452
Wachter A., Winters J. M., Schröder K. P., Sedlmayr E., 2008, A&A, 486, 497

This paper has been typeset from a TEX/LATEX file prepared by the author.

Downloaded from https://academic.oup.com/mnras/article-abstract/461/1/542/2595305 by guest on 13 June 2020